

An extensive study on the influence of operational limits on voltage stability assessment ^{*}

Lucas Sales Neves ^{*} Luís Fernando Costa Alberto ^{**}

^{*} São Carlos School of Engineering, University of São Paulo, SP,
(e-mail: lucas.sales.neves@usp.br).

^{**} São Carlos School of Engineering, University of São Paulo, SP,
(e-mail: lfcaberto@usp.br).

Abstract: This work presents a comprehensive analysis of a three-bus power system regarding voltage stability concerning operational limits and their influence in the region of safe operation. Specifically, this paper describes the effect of reactive power limits both in the distance to collapse and in the occurrence of saddle-node or limit-induced bifurcations. We also describe how the bifurcation surface changes with respect to reactive power limits, as well as the effect of voltage limits. The use of static analyses to assess voltage stability is supported by dynamic simulations. The studies performed for this test system can be easily extended to analyze real power systems.

Keywords: voltage stability, load dynamics, reactive power limits, voltage limits.

1. INTRODUCTION

Voltage stability is a fundamental field of study regarding electric power systems security. The main goal of voltage stability assessment is to judge if the power system, for a specific operating point, is prone to a voltage collapse, being vulnerable to a sudden and uncontrollable variation on voltage levels. Even though this problem has been discussed thoroughly in the literature (for example, Taylor (1994); Van Cutsem and Vournas (1998)), this paper presents some insights that may support voltage stability analyses.

Some contributions of this paper are:

- We investigate how reactive power limits influence not only the type of the occurring bifurcation but also the distance to this bifurcation.
- We present a clear correspondence between static and dynamic analyses in relation to voltage stability.
- We provide the quantitative and qualitative distinction of the mechanisms involved in voltage collapse in relation to saddle-node bifurcations and limit-induced bifurcations.

To present the voltage instability problem in a clear way, a small three-bus power system is studied. Albeit simple, this small system presents the main issues of large power systems in relation to voltage stability, such as:

- the inability of the generation and transmission systems to meet the power demanded by the load;
- the voltage collapse due to the loss of an equilibrium point when parameters are slowly varied.

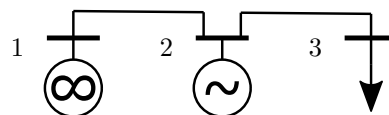


Fig. 1. The three-bus system.

2. THE STUDIED TEST-SYSTEM

In this paper, the three-bus power system shown in Figure 1 is analyzed, which is composed of one infinite bus (bus 1), one generation bus (bus 2) and one load bus (bus 3). Both transmission lines shown in Figure 1 have a series resistance of 0.2 pu, a series reactance of 1 pu and a (total) shunt susceptance of 0.02pu. The voltage at bus 1 is maintained at 1 pu.

In our study, the traditional steady-state generator model is used for bus 2. More precisely, this bus is modelled as a “PV” bus while its reactive power is within limits, and the bus is modelled as a “PQ” bus when reactive power limits are reached. The voltage setpoint value for this generator is 1 pu, and different values of reactive power limits are used throughout the paper. This generator is working as a synchronous condenser, i.e., it does not inject active power in the system.

We also consider that the load connected to bus 3 satisfy a power-restoration dynamics. This means that the load steady-state model, governed by its equilibrium equations, can be approximated by a constant power model. Hence, bus 3 can be treated as a “PQ” bus. This approximation is valid for loads such as induction motors, loads fed by LTC transformers or thermostatic loads (Van Cutsem and Vournas (1998)).

When appropriate, a *quasi-steady-state* (QSS) simulation is performed, where the only dynamics involved refer to the load-restoration dynamics. In these simulations, the differential equations describing these dynamics are:

^{*} This work was partially supported by São Paulo Research Foundation (FAPESP) under grants 2018/24815-7, 2014/50851-0 and 2018/20104-9.

$$\frac{dG}{dt} = P_{\text{spec}} - P_{\text{load}}, \quad (1a)$$

$$\frac{dB}{dt} = Q_{\text{load}} - Q_{\text{spec}}, \quad (1b)$$

where $Y = G + jB$ is the admittance associated with the load power connected to bus 3. $P_{\text{spec}} + jQ_{\text{spec}}$ is the complex specified power for the load bus, while $P_{\text{load}} + jQ_{\text{load}}$ is the actual power demanded by the load. These equations follow a simple logic: to increase the active power P_3 , one needs to increase the conductance G_3 ; to increase the (demanded) reactive power Q_3 , one needs to decrease the susceptance B_3 . The equilibrium is reached when the power demanded by the load (given by $P_{\text{load}} + jQ_{\text{load}}$) matches the specified value (given by $P_{\text{spec}} + jQ_{\text{spec}}$).

Our main goal is to analyze the voltage profiles of the system with the variation of the load connected to bus 3. For certain values of power, the power flow solution for this three-bus system disappears. When this happens, the load dynamics described by equation (1) will lead the system to a collapse.

3. UNLIMITED REACTIVE POWER RESERVE

Firstly, consider that the synchronous condenser can maintain the voltage at bus 2 at its setpoint value despite the reactive power output of the machine. In this situation, the power flow equations are:

$$P_{\infty} - P_{12}(E_1, E_2) = 0, \quad (2a)$$

$$Q_{\infty} - Q_{12}(E_1, E_2) = 0, \quad (2b)$$

$$P_{\text{gen}} - P_{21}(E_1, E_2) - P_{23}(E_2, E_3) = 0, \quad (2c)$$

$$Q_{\text{gen}} - Q_{21}(E_1, E_2) - Q_{23}(E_2, E_3) = 0, \quad (2d)$$

$$-P_{\text{load}} - P_{32}(E_2, E_3) = 0, \quad (2e)$$

$$-Q_{\text{load}} - Q_{32}(E_2, E_3) = 0, \quad (2f)$$

$$E_1 - E_{\infty} = 0, \quad (2g)$$

$$|E_2| - V_{\text{spec}} = 0, \quad (2h)$$

where:

- E_1, E_2 and E_3 are the complex voltages at buses 1, 2 and 3, respectively.
- $P_{12} + jQ_{12}$ and $P_{21} + jQ_{21}$ are the complex power flowing through both sides of the transmission line connecting buses 1 and 2, computed from variables E_1 and E_2 , besides the line parameters. Similarly, $P_{23} + jQ_{23}$ and $P_{32} + jQ_{32}$ represent the power flowing through the other transmission line.
- $P_{\infty} + jQ_{\infty}$ is the complex power injected by the infinite bus in the system.
- $P_{\text{gen}} + jQ_{\text{gen}}$ is the complex power injected at bus 2 by the generator. From Section 2, $P_{\text{gen}} = 0$.
- $P_{\text{load}} + jQ_{\text{load}}$ is the power demanded at the load bus. This is the same variable as in (1).
- E_{∞} is the specified voltage for the infinite bus. From Section 2, $E_{\infty} = 1 + j0$.
- V_{spec} is the setpoint voltage for the synchronous condenser. From Section 2, $V_{\text{spec}} = 1$.

This set of 9 real equations (recall that (2g) is a complex equation) and 9 real variables (variables E_1, E_2 and E_3 are complex, while variables P_{∞}, Q_{∞} and Q_{gen} are real) can be solved given the power $P_{\text{load}} + jQ_{\text{load}}$ at the load bus. For example, when $P_{\text{load}} + jQ_{\text{load}} = 0$, one power flow solution is:

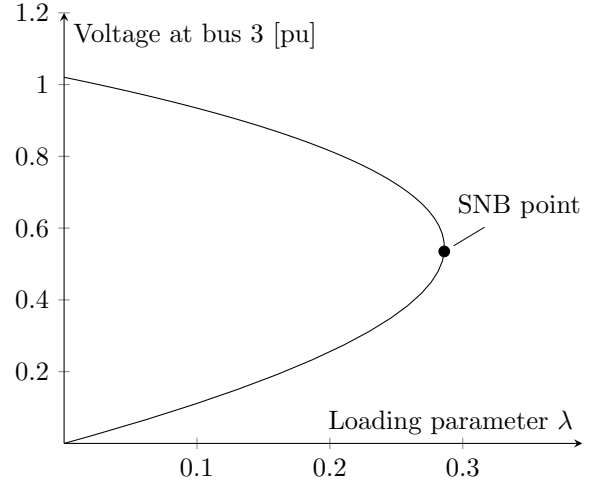


Fig. 2. Nose curve for bus 3.

$$E_1 = 1 + j0,$$

$$E_2 \approx 1 / \angle -0.00496^\circ,$$

$$E_3 \approx 1.02 - j0.00425,$$

$$P_{\infty} + jQ_{\infty} \approx 8.33 \times 10^{-5} - j0.0200,$$

$$Q_{\text{gen}} \approx -0.0604.$$

Note that the voltage at bus 3 is larger than 1 pu, due to the shunt elements of the transmission lines.

Now, consider that the load connected to bus 3 gradually increases following the pattern given by:

$$P_{\text{load}} + jQ_{\text{load}} = (0.8 + j0.6)\lambda. \quad (3)$$

For this pattern, the power flow solution can be tracked with the variation of λ (this procedure is usually referred to as continuation power flow (Iba et al. (1991); Ajjarapu and Christy (1992); Canizares and Alvarado (1993); Chiang et al. (1995))). The so-called “nose curves” present a graphical visualization of how the solution point varies with λ . A nose curve for bus 3 is shown in Figure 2.

Observe that there is a maximum value for λ (given by $\lambda_{\text{max}} \approx 0.286$) for which the power flow equations have a solution. After this value, the power system dynamic model (the QSS model, which combines equations (1) and (2)) do not have an equilibrium point. The point where the system loses the equilibrium is known as a saddle-node bifurcation point (Seydel (2010)). At the SNB point, the Jacobian matrix of the power flow equations becomes singular.

For an example of a stable loading variation, assume that the load suddenly increases from $\lambda = 0$ to $\lambda = 0.2$. Starting from the equilibrium for $\lambda = 0$, the solution of the differential-algebraic equations (DAE) when $P_{\text{spec}} + jQ_{\text{spec}} = 0.2 \times (0.8 + j0.6)$ is shown in Figure 3 and Figure 4.

An unstable loading variation occurs if λ becomes greater than λ_{max} , despite how small this variation is. Starting from the equilibrium for $\lambda = 0.28621 < \lambda_{\text{max}}$, the solution of the differential-algebraic equations when $P_{\text{spec}} + jQ_{\text{spec}} = 0.28622 \times (0.8 + j0.6)$ (where $0.28622 > \lambda_{\text{max}}$) is shown in Figure 5 and Figure 6. Note that, in spite of

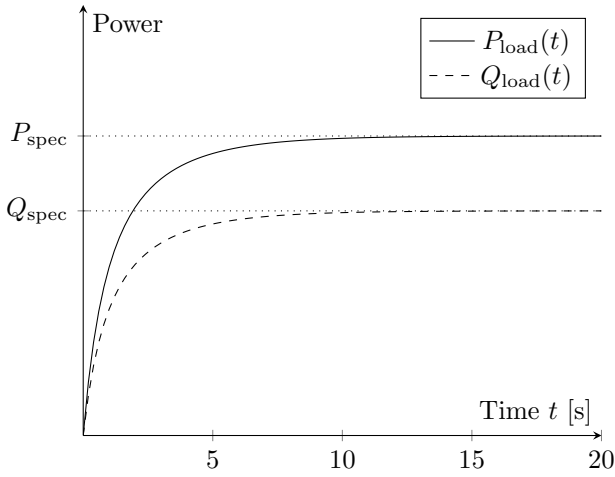


Fig. 3. Power demanded at the load bus.

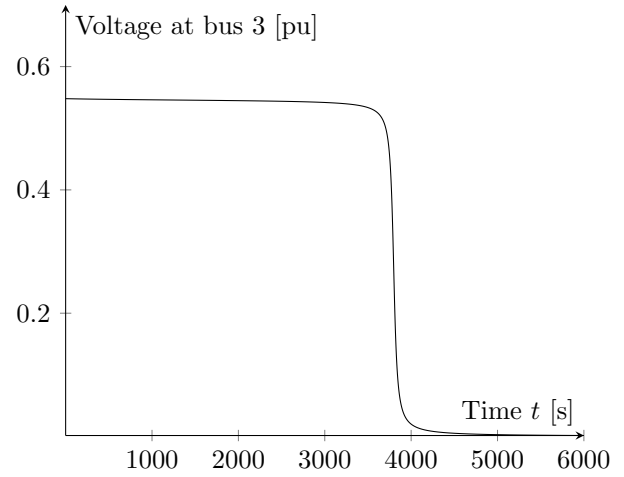


Fig. 6. Voltage collapse.

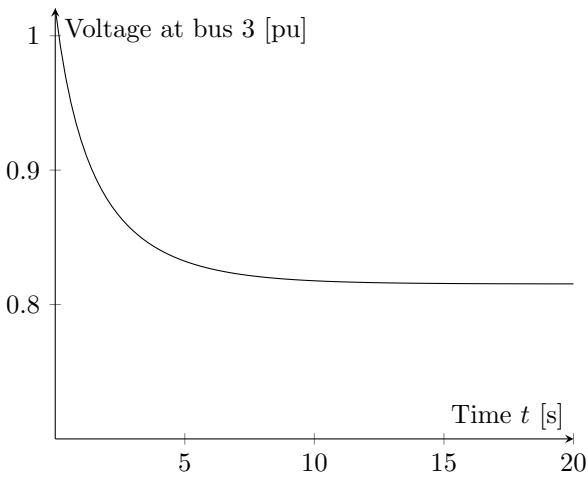


Fig. 4. Voltage at the load bus.

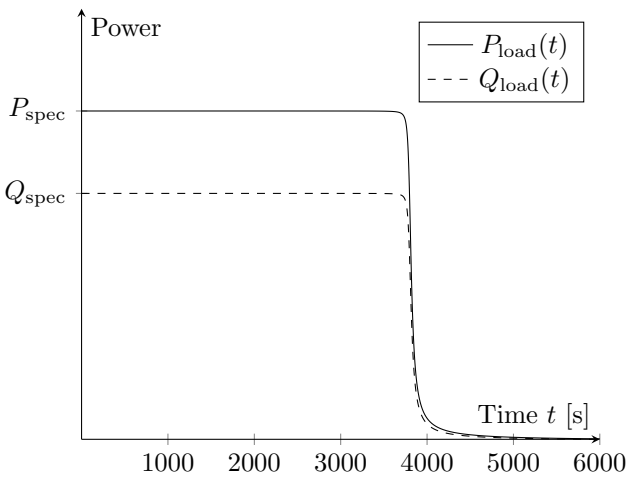


Fig. 5. Power demanded at the load bus.

the form of Figures 5 and 6, this is an unstable situation because the values of G and B (of (1)) grow indefinitely.

The small variation from $\lambda = 0.28621$ to $\lambda = 0.28622$ was sufficient to cause a voltage collapse, as shown in Figure 6. Even though the fast voltage decrease only occurs after $t = 3000$ s, the unstable situation was present from

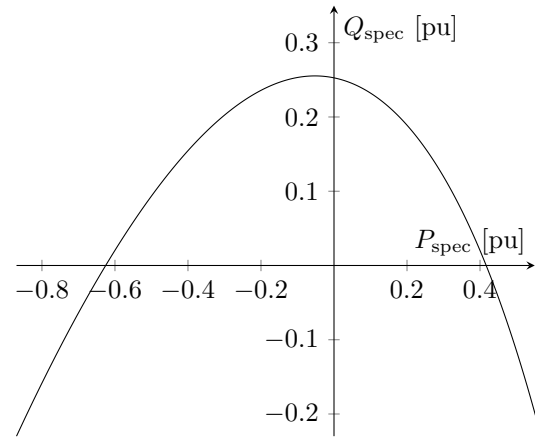


Fig. 7. Bifurcation surface.

the very beginning. The difference from a slow and fast dynamics in this unstable trajectory is due to the fact that the initial point is near the SNB point shown in Figure 2 (Dobson and Chiang (1989)). Note that the values of $P_{load}(t)$ and $Q_{load}(t)$ are always less than the specified values P_{spec} and Q_{spec} , despite how close they are to P_{spec} and Q_{spec} for $t \leq 3000$ s.

Up to this point, we have analyzed voltage stability constrained to a pattern of load variation shown in (3). However, parameters P_{spec} and Q_{spec} do not necessarily vary together. In general, parameters are independent from each other, and for each loading variation pattern (similar to the one in (3)), one specific value of λ_{max} is calculated and a corresponding bifurcation point $(P_{spec}(\lambda_{max}), Q_{spec}(\lambda_{max}))$ is obtained.

By changing the direction of load variation in equation (3) and computing their respective bifurcation points, one obtains the curve shown in Figure 7. This is a (one-dimensional) curve because the system has two parameters, namely P_{spec} and Q_{spec} . In general, however, when we have n parameters, the set of bifurcation points is a $(n - 1)$ -dimensional surface.

(P_{spec}, Q_{spec}) points below the curve in Figure 7 admit a power flow solution, while this solution disappears on the curve. By further analyses, we verify that no Hopf

bifurcation occurs in this system, which indicates that the equilibrium point at $P_{\text{spec}} + jQ_{\text{spec}} = 0$ remains stable when these parameters are varied.

4. LIMITED REACTIVE POWER RESERVE

In practice, generators can only control its voltage as long as the limits in the machine's capability curve are satisfied. When these limits are reached, the generator loses the ability to control the voltage, and its reactive power is fixed at the reached limit.

The upper limit is reached when the system is demanding more reactive power. The generator loses the ability to control the voltage when there is a shortage of reactive power, and since the transmission system is mainly inductive, voltages are expected to drop. On the other hand, the violation of the lower bound means that there is a surplus of reactive power in the system, so voltages are expected to rise near the generator. This discussion justify the following steady-state generator model:

$$\begin{cases} Q = Q_{\max}, & \text{if } V < V_{\text{spec}}, \\ Q_{\min} \leq Q \leq Q_{\max}, & \text{if } V = V_{\text{spec}}, \\ Q = Q_{\min}, & \text{if } V > V_{\text{spec}}. \end{cases} \quad (4)$$

Previously, the generator was modelled by (2h). When reactive power limits are included, (2h) is replaced by (4), while the other equations remain the same. Note that $V = |E_2|$ and $Q = Q_{\text{gen}}$ when the model (4) is included to the power flow equations in (2).

For illustration purposes, consider that $Q_{\min} = 0.1$ and $Q_{\max} = 0.2$. The pattern in (3) is used again to generate the nose curve shown in Figure 8. This figure shows three situations with the increase of λ :

- Initially, when the load is small, the reactive power of the generator is held at the lower limit. As a result, its voltage is larger than $V_{\text{spec}} = 1$, in accordance with (4).
- With the increase of the load, the generator voltage decreases, until it finally reaches the specified value. Starting at this point, the generator starts to regulate its voltage, while its reactive power starts to increase.
- By further increasing λ , the upper limit of reactive power is reached, and the generator voltage starts decreasing again, according to (4). λ continues to increase, and a SNB point occurs when the generator is modelled as $Q = Q_{\max}$.

Dynamic simulations by integrating the QSS model are similar to the previous section. In this case, however, one may expect cusp points in the simulation due to the change in model due to (4). For example, when suddenly increasing λ from 0 to 0.2, Figure 8 shows that the generator model changes from $Q = Q_{\min}$ to $V = V_{\text{spec}}$. The dynamic simulation for $P_{\text{spec}} + jQ_{\text{spec}} = 0.2 \times (0.8 + j0.6)$ starting from the equilibrium point for $P_{\text{spec}} + jQ_{\text{spec}} = 0$ is depicted in Figure 9, which shows that the change in the generator model occurs at $t \approx 2.27$ s.

Now, consider $Q_{\max} = 0.45$, which generates the nose curve in Figure 10. Note that the generator can regulate its terminal voltage for longer in comparison with Figure 8. However, the equilibrium point disappears as soon as the

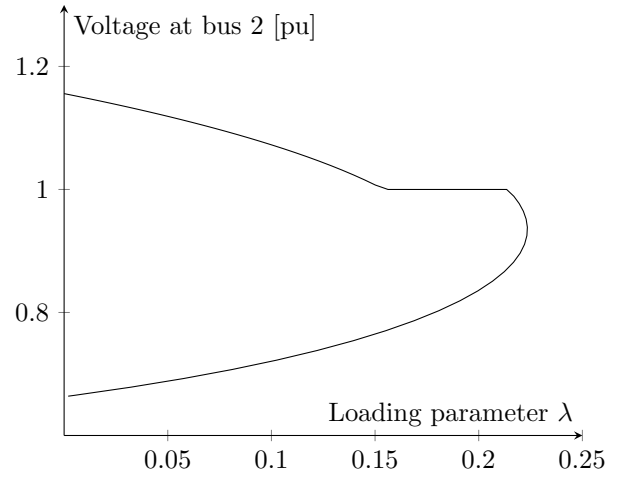


Fig. 8. Nose curve for bus 2.

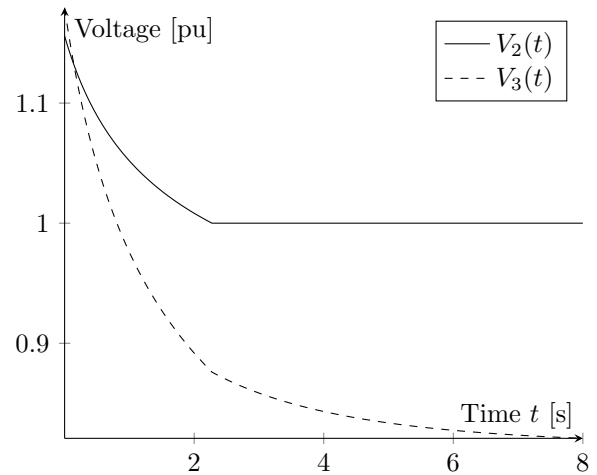


Fig. 9. Change in the generator model.

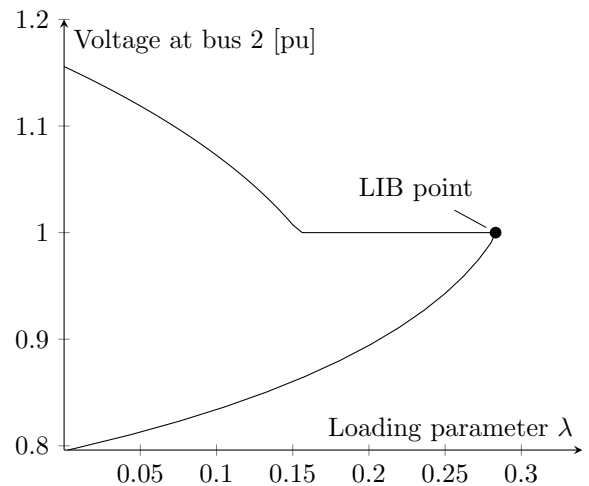


Fig. 10. Occurrence of a Limit-Induced Bifurcation.

generator model changes from $V = V_{\text{spec}}$ to $Q = Q_{\max}$. When the equilibrium point disappears at the moment that a device reaches its limit, we say that the system undergoes a limit-induced bifurcation (LIB) (Dobson and Lu (1992)).

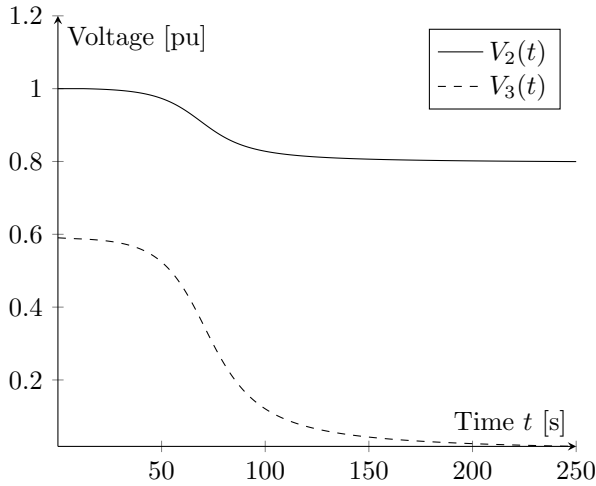


Fig. 11. Voltage profile after a LIB.

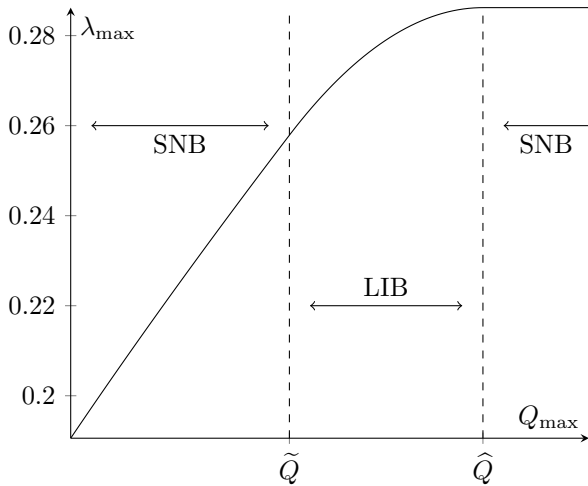


Fig. 12. Distance to collapse as a function of the upper reactive power limit.

Figures 5 and 6 showed the impact of a SNB on the power system. In comparison, Figure 11 highlights the effect of a LIB. Note that the distinction of the “slow” and “fast” dynamics are less clear in the case of a LIB because, in the case of LIB, there is no slow (center) manifold governing the unstable dynamics. The simulation in Figure 11 shows the result of integrating the QSS model for $\lambda = 0.285 > \lambda_{\max}$ starting from the equilibrium for $\lambda = 0.284 < \lambda_{\max}$.

When Q_{\max} increased from 0.2 to 0.45, the value of λ_{\max} in (3) increased, while the bifurcation type changed from SNB to LIB. One may expect that further increasing Q_{\max} will continue to increase λ_{\max} (with a larger reactive power reserve, the system can withstand bigger loads). Actually, if Q_{\max} is too large, the system will behave as if there were no upper limit, which will result in the SNB shown in Figure 2. We next investigate the value of λ_{\max} as a function of Q_{\max} and the transition from SNBs to LIBs and vice-versa. The results are reported in Figure 12.

The transition point between a SNB and a LIB occurs when the SNB point for the generation modelled as $Q =$

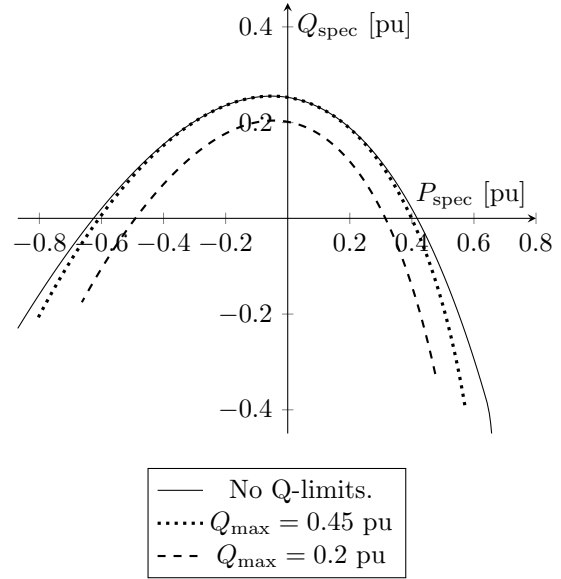


Fig. 13. Influence of Q-limits on the bifurcation surface.

Q_{\max} occurs exactly for $V = V_{\text{spec}}$. This occurs for $\tilde{Q} \approx 0.311$ pu.

The transition point between a LIB and a SNB occurs when the upper limit is never reached at all. This occurs when Q_{\max} is greater than the reactive power at the bifurcation point of Figure 2, given by $\hat{Q} \approx 0.498$ pu.

Lastly, we draw the bifurcation surface for the system with limited reactive power reserve and compare it with the original bifurcation surface (shown in Figure 7) in Figure 13. This figure clearly shows how reactive power limits have an impact on the distance to collapse, which is intuitive: since less reactive power can be transferred by the system, less reactive power can be demanded by the load. Recall that points below the bifurcation surface are feasible points, for which the DAE has a stable equilibrium point.

Note that the bifurcation surface with no Q-limits and the bifurcation surface with $Q_{\max} = 0.45$ pu share some bifurcation points. This occurs for load variation patterns such that the generator reactive power never reaches 0.45 pu.

5. INFLUENCE OF VOLTAGE LIMITS

Next, voltage limits are included in the power flow model. Together with the bifurcation surface, voltage limits delimit the region of safe operation for the power system. The system does not become unstable when a voltage limit is violated, but this limit can indirectly lead to an unstable situation due to the protection system. For example, if the voltage at a generator becomes unacceptably low, the protection system might disconnect the generator from the power system, and this sudden reduction in the power transfer capability may lead to a voltage collapse.

To simplify the analysis, we consider only the upper bound for the voltage at the load bus, given by 1.05 pu. Our goal is to determine which values of $P_{\text{spec}} + jQ_{\text{spec}}$ violate this upper bound.

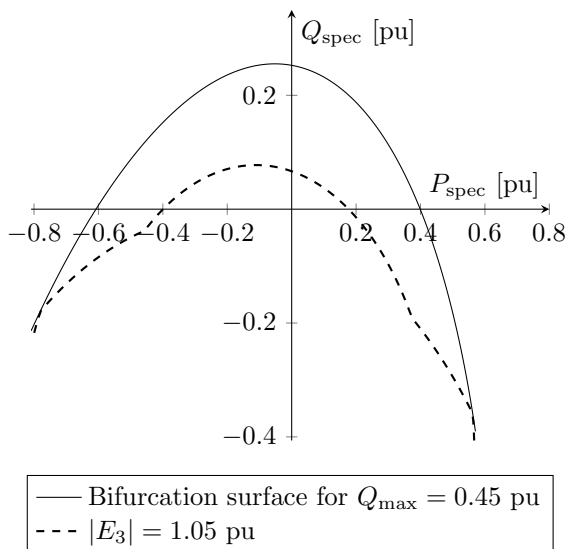


Fig. 14. The region of safe operation for $P_{\text{spec}} + jQ_{\text{spec}}$.

With only one voltage limit, $P_{\text{load}} + jQ_{\text{load}}$ can replace E_3 as a complex variable in (2). We fix $|E_3| = 1.05$ pu and we compute the solution of (2) for different values of $\angle(E_3)$. The value of $P_{\text{load}} + jQ_{\text{load}}$ in these solution points are, in fact, the values of P_{spec} and Q_{spec} for which $|E_3| = 1.05$ pu.

As in the previous section, (2h) is replaced with (4), and for this section the values $Q_{\min} = 0.1$ pu and $Q_{\max} = 0.45$ pu are adopted. The set of points $(P_{\text{spec}}, Q_{\text{spec}})$ such that $|E_3| = 1.05$ pu is drawn together with the bifurcation surface in Figure 14. The region between these two curves is the region for which the power system admits a stable solution point satisfying $|E_3| \leq 1.05$ pu. From this figure, power system operators can examine how far the system is from a collapse.

6. CONCLUSIONS

This paper presented an extensive voltage stability analysis of a three-bus power system, explaining the mechanisms that can lead the system to a voltage collapse.

This paper clearly presents the effects of reactive power limits in voltage stability, regarding both the distance to collapse and the possibility of SNBs and LIBs. The influence of these limits on the bifurcation surface is also studied. Moreover, static analyses are accompanied by dynamic simulations that corroborate the use of static tools to assess voltage stability.

Even though a small power system is analyzed, this paper presents the methodologies used in model-based voltage stability assessment of real, large power systems, providing insights in the effects of operational limits in the search for bifurcations.

REFERENCES

Ajjarapu, V. and Christy, C. (1992). The continuation power flow: a tool for steady state voltage stability analysis. *IEEE Transactions on Power Systems*, 7(1), 416–423. doi:10.1109/59.141737.

Canizares, C.A. and Alvarado, F.L. (1993). Point of collapse and continuation methods for large AC/DC systems. *IEEE Transactions on Power Systems*, 8(1), 1–8. doi:10.1109/59.221241.

Chiang, H.D., Flueck, A.J., Shah, K.S., and Balu, N. (1995). CPFLOW: a practical tool for tracing power system steady-state stationary behavior due to load and generation variations. *IEEE Transactions on Power Systems*, 10(2), 623–634. doi:10.1109/59.387897.

Dobson, I. and Lu, L. (1992). Voltage collapse precipitated by the immediate change in stability when generator reactive power limits are encountered. *IEEE Transactions on Circuits and Systems I: Fundamental Theory and Applications*, 39(9), 762–766. doi:10.1109/81.250167.

Dobson, I. and Chiang, H.D. (1989). Towards a theory of voltage collapse in electric power systems. *Systems & Control Letters*, 13(3), 253–262. doi:10.1016/0167-6911(89)90072-8.

Iba, K., Suzuki, H., Egawa, M., and Watanabe, T. (1991). Calculation of critical loading condition with nose curve using homotopy continuation method. *IEEE Transactions on Power Systems*, 6(2), 584–593.

Seydel, R. (2010). *Practical Bifurcation and Stability Analysis*. Interdisciplinary Applied Mathematics. Springer-Verlag New York, 3 edition. doi:10.1007/978-1-4419-1740-9.

Taylor, C. (1994). *Power System Voltage Stability*. McGraw-Hill, Singapore, 1 edition.

Van Cutsem, T. and Vournas, C. (1998). *Voltage Stability of Electric Power Systems*. Power Electronics and Power Systems. Springer, Boston, MA, 1 edition. doi:10.1007/978-0-387-75536-6.